SPECIFIC FEATURES OF IONOSPHERIC DISTURBANCES ACCOMPANYING THE 14–20 JANUARY 2022 MAGNETIC STORM

© 2025 V. I. Kurkin*, N. A. Zolotukhina, S. N. Ponomarchuk***, A. V. Oinats****, K. G. Ratovsky*****

Institute of Solar-Terrestrial Physics of Siberian Branch of Russian Academy of Sciences (ISTP SB RAS), Irkutsk, Russia

**e-mail: vikurkin@yandex.ru*

***e-mail: zolot@iszf.irk.ru*

****e-mail: spon@iszf.irk.ru*

*****e-mail: oinats@iszf.irk.ru*

******e-mail: ratovsky@iszf.irk.ru*

Received February 14, 2024

Revised May 06, 2024

Accepted July 25, 2024

Abstract. We conducted the analysis of ionospheric disturbances that occurred during the moderate magnetic storm of 14–20 January 2022. The study is based on data of vertical and oblique ionospheric sounding obtained in the Northeastern region of Russia, and supplemented by observations at HF radars and magnetic observatories. It has been revealed that the amplitudes of positive and negative ionospheric disturbances accompanying this storm are comparable to those observed on other days of January during weak magnetic storms and disturbances. Specific features of the disturbances observed only during the storm in question are as follows: (1) a midnight–morning increase of the maximum observed frequency of one-hop mode of HF radio wave propagation on the paths Norilsk — Tory and Magadan — Tory on 14 January; (2) enhanced nighttime fluctuations in F2-layer critical frequency in Irkutsk and the maximum observed frequency of one-hop mode on the path Magadan — Tory on 15 January; (3) Morning–midday *Es* layers with limiting frequencies reaching 7 MHz that were observed in mid-latitudes at the end of the first and beginning of the second day of the storm recovery phase.

DOI: 10.31857/S00167940250609e6

1. INTRODUCTION

Studies of the influence of solar and geomagnetic activity on the conditions of radio wave propagation, started in the late 20s of the last century [Pickard, 1927; Anderson, 1928], made it possible to establish a close connection between geomagnetic disturbances and significant changes in the structure of the ionosphere. Based on the results of these studies, the term "ionospheric storm" was introduced, which is understood as a set of ionospheric disturbances accompanying geomagnetic storms. At present, the study of ionospheric storms is developing very intensively in both observational and theoretical directions. Interest in this phenomenon is due to the fact that ionospheric disturbances often disrupt the operation of ionospheric radio communication systems, causing interference, and in extreme cases, the lack of radio wave passage between the receiving and transmitting devices, as well as energy systems, leading to partial or complete power outages, failures in the operation of railway automation, etc. [Goodman et al. [Goodman et al., 2006; Kuznetsov, 2014; Pilipenko, 2021].

To study the spatial and temporal dynamics of an ionospheric storm, it is customary to use the difference between the current and background values of the critical frequency of the F2 layer of the ionosphere (*foF2*) or the maximum electron concentration of the ionosphere $NmF2 = 1.24 \times 10^4 (foF2)^2$, as well as between the current and background values of the total electron content (TEC). According to the sign of the indicated difference, ionospheric disturbances are divided into positive and negative disturbances, which are considered to be the basic elements of an ionospheric storm. The average values of *foF2/PES* measured on the nearest magnetically quiet days (*q*-days) to the beginning of the storm or their monthly median values are usually used as background values [Danilov, 2013; Mikhailov et al., 2004]. However, significant changes in ionospheric parameters, comparable to the changes occurring during storms, are observed even on *q*-days, which requires checking the legitimacy of using these days to determine the background in each case [Perrone et al., 2020]. The second method is more acceptable when the foF2/PES values measured on magnetically calm days differ significantly from their monthly median values. In addition to positive and negative disturbances of different amplitude and duration, an ionospheric storm includes enhanced formation of sporadic and diffuse ionospheric layers.

The spatial and temporal extent and intensity of ionospheric disturbances, as well as the level of geomagnetic activity, increase with the growth of corpuscular and electromagnetic energy coming from the interplanetary medium initially to the high-latitude part of the magnetosphere-ionosphere system and then to other regions of the outer geospheres [Prölss, 2006]. The strongest magnetosphere-ionosphere perturbations occur in the years of solar activity maximum.

The generalized spatial and temporal picture of ionospheric storm development is based mainly on data obtained during isolated strong and moderate magnetic storms that have clearly

pronounced main, recovery, and in some cases, initial phases [Prölss, 1997; Fuller-Rowell et al., 1997; Buonsanto, 1999; Mendillo, 2006; Danilov, 2013]. It has been found that ionospheric storm manifestations registered by a particular ionosonde depend not only on interplanetary, magnetospheric, and thermospheric processes, but also on the location of the observation point and its local time [Zherebtsov and Pirog, 2008; Kurkin et al., 2008].

Much less information has been collected to date on the ionospheric perturbations accompanying weak magnetic storms, which at mid-latitudes can be comparable to the changes during strong magnetic storms [Buresova et al., 2014]. The decrease in the maximum observed frequencies of the maximum observed frequencies of the single-skewed mode of SW radio wave propagation (MSF1*F2*) during weak magnetic storms can be 25-50 % [Kurkin et al., 2022; Kurkin et al., 2022]. In [Ratovsky et al, 2022] showed that about half of the 25 extreme increases of the maximum electron concentration in the *F2*-layer of the ionosphere observed in Irkutsk in 2003-2016, at which the normalized deviations of *NmF2* from the monthly median values were greater than 150 %, were observed during weak geomagnetic disturbances with minimum $Dst > -30$ nTl. According to the criterion specified in [Gonzalez et al., 1994], perturbations with the *Dst* index > – 30 nTL are not geomagnetic storms.

An attempt to statistically study the response of the ionosphere to "weaker" ("weaker") geomagnetic activity was made in [Chen et al., 2022]. To select "weaker" events, the authors used the criterion $Ap < 60$. As a result of applying this criterion, the sample analyzed in [Chen et al., 2022] included strong and moderate magnetic storms, which casts doubt on the validity of the conclusions made in this work about the trends in the ionospheric response to weak magnetic perturbations. Another significant drawback of the work [Chen et al., 2022], which puts its conclusions in doubt, is the heterogeneity of the experimental data on which it is based.

In this paper we continue the studies of the ionospheric response to weak magnetic storms started in [Kurkin et al., 2022; Kurkin et al., 2022], where it is shown that the ionospheric response to the impact of a high-velocity solar wind flow causing a storm depends both on the geoeffective parameters of the flow and on the duration of its impact on the magnetosphere-ionosphere system and its initial state.

2. OBJECT AND PURPOSE OF THE STUDY

The ionospheric data obtained in January 2022 at the growth phase of the 25th solar activity cycle were selected for the study. The analysis of the geomagnetic situation is based on the series of values of *Kp*, *Dst, ap* [URL OMNI2], and *SME* [URL SME] indices. The characteristics of the interplanetary sources that caused the geomagnetic perturbations are presented in the paper by the solar wind (SW) and interplanetary magnetic field (IMF) plasma parameters [URL OMNI2]. The

Akasofu parameter ε (the energy flux falling from the interplanetary medium onto the sunlit magnetosphere [Akasofu, 1981]) was calculated from the SW and IMF parameters.

Fig. 1.

Fig. 1 shows that during the selected month, the magnetosphere-ionosphere system was exposed to 4 high-velocity solar wind streams with peak velocities greater than 450 km/s. The first flux caused weak disturbances on January 1-4 with a minimum of *Dst* = – 25 nTL and a maximum of *Kp* = 4; the second, slower flux on January 8-11, − a weak storm on January 8-11 with an increase in *Kp* to the storm level *Kp* = 5 and a decrease in *Dst* to -27 nTL.

The disturbances of January 14-20 are a moderate magnetic storm (minimum *Dst* = –91 nTL, maximum *Kp* = 6-). It was caused by a complex interplanetary inhomogeneity formed by an interplanetary coronal mass ejection, a high-speed solar wind flow from the coronal hole *CH1054*, and two other coronal ejections. The wind speed increased non-monotonically from 360 km/s in the leading part of the inhomogeneity to 700 km/s on the penultimate day of the storm. At the leading front of the inhomogeneity, the southward-directed vertical component of the interplanetary magnetic field (BzMMP) intensified to -17 nT (not shown in the figure). Panel (*b*) shows that the power of the external source of the January 14-20 storm, estimated using the Akasofu parameter (ε), was ~ 2 times greater than the power of the interplanetary sources of other disturbances. It should be expected that this storm was accompanied by stronger ionospheric perturbations than those observed during other events.

The series of weak perturbations on 22-23 and 25-31 January were characterized by multiple decreases of *Dst*, of which only 2 can be attributed by the minima of *Dst* = -34 and -44 nT (25 and 31 January, respectively) to weak magnetic storms.

Note that in January 2022 of the sudden stratospheric warming, which has, according to Mikhailov et al. [2021], there was no appreciable influence on the development of ionospheric disturbances [Vargin et al., 2022]. But at ~ 04:15 UT on January 15, there was a powerful eruption of Tonga volcano, which caused the generation of moving ionospheric disturbances (MID) with main periods of ~ 10-30 min, propagating along the great circle at a speed of 300-350 m/s [Zhang et al., 2022].

The specific purpose of our work is to compare the ionospheric disturbances that developed during the moderate storm on January 14-20 with those disturbances observed on other days of January 2022, including days of weak storms and q-days.

3. ANALYZED DATA

The study is based on a series of monthly values of the critical frequency and peak height of the *F2*-layer (*foF2* and *hmF2*), the limiting frequency of the *Es*-layer (*foEs*), as well as measurements of the MHF1*F2* obtained on the traces of inclined sounding (IS) of the ionosphere.

The values of foF2*,* *hmF2*, *foEs* were measured with the DPS-4 ionosonde and LFM ionosonde located in Irkutsk (52.5° N, 104° E, Φ = 48.4°) with Δt = 15 min and in Tora, p. Buryatia (52° N, 103° E, Φ = 48°) with a frequency Δt = 1 min. Here Φ is the corrected geomagnetic latitude. Additionally, we use observations of the auroral echo in Yekaterinburg (*ECW*) and Magadan (*MGW*) on SW radars, series of values of the horizontal (*H*) component of the geomagnetic field measured at the observatories Irkutsk, Yakutsk (62° N, 129.7° E, Φ = 56.8°) [URL Intermag] and the original data of the magnetic observatory Norilsk (69.4° N, 88.1° E, Φ = 65.3°), as well as the coordinates of the polar and equatorial boundaries of the auroral oval taken at the site [URL Oval]. A map of the location of the observing facilities is shown in Fig. 2.

Fig. 2.

The TPLF1*F2* measurements were carried out with a frequency Δt = 5 min on the Norilsk-Tory and Magadan-Tory traces (the coordinates of the midpoints of the traces are 60.9° N, 98° E*,* Φ = 57° and 58.5° N, 125.8° E, Φ = 53.7°, respectively).

Continuous monitoring along these routes was carried out using the equipment of the multifunctional LFM ionosonde "Ionosonde-MS" [Podlesny et al. [Podlesny et al., 2013]. The northern section of the first trace is located in subauroral latitudes. The Magadan-Tory trace belongs to mid-latitudes, but during strong magnetic perturbations its northern section, including the midpoint, can be located in the area of the main ionospheric failure (MIF) [Polekh et al., 2016]. In our work, the corrected geomagnetic latitude (Φ) of the bottom of the ISU is determined using the model presented in [Deminov and Shubin, 2018]. In it, the latitude of the ISU bottom is calculated from the ap-index values in the current and several (in our case, 4) preceding 3-hour intervals.

4. IONOSPHERIC STORM ON JANUARY 14–20, 2022

Fig. 3.

The three lower panels of Fig. 3 show plots of the changes in the *TPLF1F2* at the two tracks and *foF2*, *foEs* over Irkutsk, plotted from the original data obtained during the 4 days preceding the moderate storm of January 14-20 and during the storm. For convenience of comparison, the upper panel shows a plot of the *Dst*-index variation.

The magnetic storm began around 16 UT on January 14 with the main phase and continued until the end of January 20. During the magnetically quiet days preceding the storm on January 10-13, nocturnal positive ionospheric disturbances were registered at the Magadan-Tory route and in Irkutsk. At this time, the values of MHF1*F2* were by ~2 MHz and *foF2* by ~1.5 MHz greater than

the monthly median values (shown in the figure by a gray line). The authors of [Mikhailov et al., 2004] call such events "Q disturbances" and believe that they are genetically related to planetary waves. Due to the presence of nocturnal Q disturbances, we chose the monthly median values of ionospheric parameters as the background ones.

The plots shown in Fig. 3, show that in the longitudinal sector considered by us the ionospheric storm began before 19:00 UT on January 14, approximately 3 h after the beginning of the main phase of the magnetic storm, and ended 5 days later (about 14:00 UT on January 19 on the penultimate day of the late recovery phase of the storm). We shall indicate clearly visible on the diagrams perturbations, which can be manifestations of the ionospheric storm.

4.1 Positive ionospheric perturbation observed at the Norilsk-Tory route at 18:53-23:53 UT on January 14 after a 200-minute blackout, and a sharp increase of *ELF1F2* from 8 to 13.6 MHz registered at the Magadan-Tory route at 22:00-22:05 UT on January 14 (between two sounding sessions) after the negative perturbation. In Fig. 3 these elements are marked with black arrows. On the Norilsk-Tory track, the perturbation was maximum at 20:58-21:13 UT on January 14.

4.2 The daytime negative disturbance registered at the Magadan-Tory route at 23:45-04:50 UT on January 14-15 and the prolonged daytime positive disturbance developing over Irkutsk at 02:00-09:00 UT on January 15 partially overlapping with it in time are highlighted by ovals.

4.3 Strengthening of short-period variations of *MHF1F2* and *foF2* during the night hours of January 15 on the Magadan-Tory route (at 10-21 UT; 18.5-05.5 LT) and over Irkutsk (at 13-22 UT; 20-05 LT). In Fig. 3 these intervals are marked by gray rectangles on the abscissa axis of panels *c*, *d. The* average period of variations $T \approx$ 110-120 min.

4.4. Intensification of diffuse morning (gray arrow in panel *d*) and afternoon (black rectangle on the abscissa axis of panel *d*) flat sporadic layers with large limiting frequencies, the maximum values of which are equal to 7 and 5.5 MHz, respectively, observed in Irkutsk and Tory.

4.5. Oval-marked nighttime negative perturbations observed in Irkutsk and on the Magadan-Tory route on January 16 at close time intervals. At the Magadan-Tora route, the nocturnal negative perturbation changed to a weaker daytime negative perturbation that lasted until 05:00 UT on January 17.

4.6 The last noticeable ionospheric perturbation (highlighted by a gray rectangle) was observed simultaneously at the Magadan-Tora route and in Irkutsk at 09:30-13:00 UT (evening hours) on January 19. At the perturbation maximum, the current values of MHF1*F2* and *foF2* were 60 and 40 % higher than the background values, respectively.

5. DISCUSSION

To compare the elements of the ionospheric storm of January 14-20, 2022 mentioned in Section 4 with ionospheric disturbances observed on other days of this month, we separated short-period (periods $0.5 < T \leq 3.5$ h, the range of large- and medium-scale LIPs [Hunsucker, 1982]) and long-period ($36 > T > 3.5$ h) disturbances from the original data series. A bandpass filter that does not produce phase shifts was used for this procedure [Marmet, 1979]. The changes in the normalized deviations of the prolonged perturbations of MHF1*F2* and *foF2* (ΔMHF1*F2* and *ΔfoF2*) observed over a month from their background values (determined for the same periods) are shown in Fig. 4.

Fig. 4.

Let us indicate those specific elements of the ionospheric storm on January 14–20, 2022 that differ significantly from the disturbances occurring on other days.

5.1 First of all, this is the only obvious ionospheric disturbance indicated in section *4.1. that* was observed in January 2022 at the Norilsk-Tory route. It developed in the form of the increase of IHF1*F2*, which began in the main phase of the storm around 19 UT on January 14 and reached at its maximum the value of *ΔfoF2* ~ 140 % 3-6 times greater than the positive perturbations observed on other days. The left panels of Fig. 5, we can see that the growth of the IHF1*F2* began after the shift of the bottom of the ISU to a latitude lower than Φ of the midpoint of the trace. The jump-like growth of MNCh1*F2* at the Magadan-Tory trace at 22:00-22:05 UT noted together with it in section *4.1*. also occurred after the transition of the midpoint of the trace from the equatorial to the polar wall of the ISU. The analysis of the EO ionograms showed that the increase of MHF1*F2* during this period of time is determined by the multibeam propagation of mode *1F2*, as the polar wall of the ISU closely approaches to the middle reflecting region of the ionosphere of the Magadan-Tory radiotrace. In addition, an additional contribution to the increase of MNF1*F2* could be made by auroral precipitations during substorms, whose manifestations in the geomagnetic variations are shown in Fig. 5 on the right.

Fig. 5.

At the subauroral Yakutsk station, a rapid decrease of the *H* component of the magnetic field, characteristic of the explosive phase of the substorm, coincided in time with the increase of the *SME* -index by ~ 400 nTL [URL *SME*]. It began approximately 5 min after the sharp increase of the MHF1*F2* at the Magadan-Tory track. At the auroral obs. Norilsk and midlatitude obs. The negative and positive *H* perturbations, respectively, began ~ 40 min later, indicating the advance of substorm events toward the west. According to MGW-radar data, the development of the substorm was accompanied by the increase of Doppler velocities of the auroral echo to the maximum values for this storm of ± 400 m/s. The echo signals came from the sector including the Yakutsk meridian, and their sources were located in the vicinity of the equatorial boundary of the auroral oval (see Fig. 6).

North of this boundary, the velocities were directed to the west; south of it ─ to the east, toward the radar, which corresponds to the area of the enhanced western electric jet.

Fig. 6.

Fig. 7.

5.2. The second specific element of the ionospheric storm under consideration is the intensification of short-period variations of ELF1*F2* and *foF2* in the night hours of January 15, noted in section *4.3*. Fig. 7 shows that at the Magadan-Tory trace the intensification of short-period variations of ELF1*F2* (marked by an arrow with a broken line) was observed at 10-21 UT (18.*18.3 UT*). 7 shows that at the Magadan-Tory track the intensification of short-period variations of *MHF1F2* (marked by an arrow with a broken line) was observed at 10-21 UT (18.5-05.5 LT) on January 15. In this interval, the standard deviation of the ELF1*F2* was 0.8 MHz, while at the same hours on other days it was 2 times smaller, only 0.4 MHz. Above Irkutsk, the activation of short-period variations of *foF2* (marked with an arrow) occurred about an hour later - at 13-22 UT (20-05 LT). It was characterized by a standard deviation S = 0.24 MHz ~ 2.5 times larger than on other days (S = 0.1 MHz). A less significant (about 1.5 times, up to S = 0.6 MHz) amplification of short-period variations of MHF1*F2* was also observed at 10-21 UT on January 9 only on the Magadan-Tory track. This interval is also marked by an arrow with a broken line. Comparing plots, we can see that in both cases the nighttime activation of short-period components of the TPLF1*F2* variations occurred at the phase of restoration of moderate and weak magnetic storms approximately a day after the bottom of the ISU moved to the middle point of the trace.

The amplitudes of short-period variations of TPLF1*F2* and *foF2* observed in the daytime hours of January 2022 (not shown in the figure) were 3 times larger (S = 1.02 and 0.32 MHz, respectively) than the amplitudes of the night variations. They slightly changed from day-to-day, including at the transition from the magnetically quiet days on January 10-13 to the magnetically perturbed day on January 15. The average period of the observed variations T ≈ 110-120 min. It is close to the period of the PIV T = 1.8 h associated with geomagnetic storms [Ding et al., 2008]. However, the permanent character of the short-period variations of MHF1*F2* and foF2 presented in the paper does not allow us to identify them with the PIVs that occur episodically at high latitudes during geomagnetic disturbances [Hunsucker, 1982].

Fig. 8.

5.3 We also attributed to the special elements of the ionospheric storm the activation of the flat midlatitude sporadic layers indicated in section 4.4. in the morning and afternoon hours of January 15-16. The upper left panel of Fig. 8 shows that sporadic layers with *foEs* from 1 to 7 MHz were observed daily. The number of sessions in which their limiting frequencies were greater than 3.1 MHz (the upper quartile of the monthly series of *foEs* values) varied from day to day from 1 to

17. The maximum number of ionograms with *foEs* > 3.1 MHz was obtained in 17 of the 18 sessions conducted at 03:30-07:45 UT (10:30-14:30 LT) on January 16. The lower left panel of Fig. 8 shows that sporadic layer activation was only observed during these hours on January 16. The activation of the morning sporadic layers at 20:45-22:45 UT (03:45-05:45 LT) on January 15, during which the highest for January2022 limit frequencies of 5.6, 6.9 and 6.6 MHz were recorded in three consecutive sessions, can also be attributed to the peculiarities of this ionospheric storm. In the morning hours, a *foEs* value = 6.6 MHz close to that observed on January 15 was recorded only on January 02 in 1 of 96 sessions conducted on that day. It was shown in [Tang et al., 2022] that the formation of dense Es-layers at middle latitudes during geomagnetic storms can be related to the wind intensification in the mesosphere and lower thermosphere.

5.4. The specificity of the positive and negative ionospheric disturbances noted in paragraphs 4.2, 4.5 and 4.6 can be judged from the diagrams presented in Figures 4, 5, 9 and 10.

Fig. 9.

Fig. 9 shows separately positive (panel *a*) and negative (panel *b*) values of ΔMHF1F2 on the Magadan-Tory route for each day of January 2022. The time of registration of positive ΔMHF1F2 values lying above the upper quartile and negative values lying below the lower quartile of the monthly series of these parameters are shown below them. In the same format, panels (*c*) and (*d*) of Fig. 9 show the positive and negative values of *ΔfoF2* obtained in Irkutsk.

5.4.1 It can be seen that the relatively weak daytime positive perturbation with *ΔfoF2* ≤ 23 % registered in Irkutsk at 02-09 UT (09-16 LT) on January 15 (see Section *4.2*.) was earlier than the evening positive perturbation with *ΔfoF2* ~ 40 % on January 19 (see section *4.6.*) and less significant evening positive perturbations with *ΔfoF2* ~ 25-38 % observed in Irkutsk at 08-13 UT (15-20 LT) on January 25 and 27-31.

The second peculiarity of the positive *foF2* perturbation on January 15 is that it corresponds to a lowering of MHF1F2 on the Magadan-Tory track. In contrast to this, the evening positive perturbations of *foF2* on January 19, 25 and 27 are observed almost simultaneously with the evening positive perturbations of MHF1*F2* at the Magadan-Tora route. This was especially pronounced in the evening hours of January 19 during the strengthening of the field of the ring current and on January 25 during a weak magnetic storm (see Fig. 1 and Fig. 4). Judging by morphological features, the evening positive perturbations are manifestations of the twilight effect ('Dusk Effect') [Buonsanto, 1999]. Returning to Fig. 5, we see that the decrease of MHF1*F2* at the Magadan-Tory trace in the first hours of January 15 followed the crossing of the bottom of the ISU of the midpoint of the trace.

Fig. 10.

The third difference between the January 15 daytime positive perturbation and the twilight effects is shown in the upper panels of Fig. 10. It can be seen that the *foF2* values increase during the increase in the peak height of the *F2* layer (panel *a*), while in the cases of crepuscular effects (panels *b*, *c*) there is a decrease in *hmF2*.

Note that diurnal positive perturbations of *NmF2* are characteristic of mid-latitudes during the winter months [Buonsanto, 1999]. It was shown in [Paznukhov et al., 2009] that at middle latitudes the positive ionospheric perturbations observed during geomagnetic storms are delayed relative to the increase in the peak height of the F2-layer. In this case, the magnitude of the delay between the increase of *hmF2* and *foF2* is 1-2 h. In our case, it is about $\Delta t \approx 1.5$ h. The time of the onset of the positive phase of the ionospheric storm depends on the local time of the observation point at the time of the onset of the geomagnetic storm. Using the graph shown in Fig. 10 in [Paznukhov et al., 2009], we obtained that the positive ionospheric disturbance could begin in Irkutsk 8-9 h after of the storm onset, i.e., at 00-01 UT, which corresponds, as well as the value of Δt, to the results of our analysis of experimental data.

Taken together, the above differences indicate that in the daytime hours of 15.01.2022, the influence of the wind directed toward the equator prevailed in the considered longitudinal sector at midlatitudes, while in the subauroral − the ISU movements and, possibly, a change in the atmospheric composition prevailed.

5.4.2 In section *4.5*. of the previous section we noted that on 16.01.2022 the nighttime negative ionospheric disturbance was observed almost simultaneously at the Magadan-Tora route and in Irkutsk. This can be clearly seen in Fig. 3 and also in Fig. 9 (panels *b*, *d*), where this disturbance is marked by arrows. The same panels show that the negative perturbations comparable by depth and time of appearance with the negative perturbation on January 16 were observed along the Magadan-Tory route during the weak geomagnetic perturbations on January 1 and 2. In Irkutsk, the closest to it by depth negative perturbations ($\Delta foF2 \approx$ - 40%) were observed on magnetically quiet days on January 6 and 7, and by the time of appearance on January 27, 2022, during the restoring phase of a weak magnetic storm. However, on January 6, 7, the *foF2* decreases were observed in the midday and evening hours rather than at night, and the perturbation on January 27 had a much smaller depth $\Delta foF2 \approx$ -30%.

The plots shown in Fig. 10 (panels *d-e*) demonstrate the trend of *hmF2* increase during the negative ionospheric disturbances that developed over the North-Eastern region of Russia in January 2022.

6. CONCLUSIONS

The analysis of vertical and oblique sounding data obtained over the North-Eastern region of Russia in January 2022 showed that the ionospheric storm accompanying the magnetic storm of January 14-20, 2022 contained the following elements not observed on other days of this month.

1. A prolonged increase of MHF1*F2* on the Norilsk-Tory track, which began on January 14 in 3 h after the beginning of the main phase with the increase of MHF1*F2* relative to the background by 100% and, after 2 h, by ΔMHF1*F2* = 120%.

2. A sharp, occurring between 2 sounding sessions at the Magadan-Tory route, increase of the ELF1*F2* at 5.6 MHz (by ~ 70%). It was registered on January 14 6 h after the beginning of the main phase.

3. activation of *foF2* and *MNCh1F2* disturbances with periods of 0.5- 3.5 h, observed over Irkutsk and on the Magadan-Tora route in the night hours of January 15 (the first day of the recovery phase of the storm).

4. Sporadic layers with large limiting frequencies continuously recorded in Irkutsk during 4 daytime hours on January 16 (the second day of the recovery phase of the storm).

Events 1 and 2 could be related to the position of the midpoints of the radiotraces relative to the polar and equatorial "walls" of the ISU. At the polar wall of the ISU, i.e., in the zone of diffuse precipitations, the concentration of electrons is increased during geomagnetic perturbations. The sharp increase of *MNCh1F2* at the Magadan-Tory trace could be connected with a substorm, which made an additional contribution to the flux of precipitating electrons. The substorm was registered at the subauroral obs. Yakutsk, located near the middle point of the Magadan-Tora trace.

The reasons for the intensification of *MHF1F2* and *foF2* fluctuations on January 15 and the formation of midlatitude sporadic layers on January 15-16 are not quite clear. Based on satellite data obtained near the L1 libration point, we believe that the intensification of nocturnal disturbances with periods of 0.5-3.5 h in the recovery phase of the storm could be related to the intensification of the thermospheric wind and the impact of fluctuations of the solar wind pressure and the interplanetary magnetic field on the magnetosphere-ionosphere system, which is in a metastable state.

The prolonged positive perturbation observed in Irkutsk in the daytime hours of January 15 developed at the background of the increase of the height of the maximum of the F2-layer and the negative ionospheric perturbation at the Magadan-Tora route. In aggregate, this indicates that in the daytime hours of 15.01.2022 in the considered longitudinal sector at middle latitudes, the influence of the wind directed to the equator prevailed at mid-latitudes, and in the subauroral sector - the displacement of the bottom of the ISU to the latitude of the midpoint of the Magadan-Tora trace and the change of the atmospheric composition.

ACKNOWLEDGEMENTS

The results were obtained on the basis of observations carried out using the equipment of the Angara Collaboration Center (http://ckp-angara.iszf.irk.ru/). We thank the managers of the sites (https://wdc.kugi.kyoto-u.ac.jp/qddays/index.html), (https://intermagnet.org), (https://cdaweb.gsfc.nasa.gov/cdaweb/istp_public), (https://ssusi.jhuapl.edu/gal_edr-aur_cs) and the SuperMAG Collaboration (https://supermag.jhuapl.edu/indices/) for the opportunity to use the information on their sites.

FUNDING

The research was financially supported by the Ministry of Education Science (grant No. 075-GZ/C3569/278).

REFERENCES

1. *Danilov A.D.* Response of the F region to geomagnetic disturbances (review) // Heliogeophysical studies. Issue 5. P. 1–33. 2013. http://vestnik.geospace.ru/index.php?id=189

2. *Deminov M.G., Shubin V.N.* Empirical model of the position of the main ionospheric trough // Geomagnetism and Aeronomy. V. 58. No. 3. P. 366–373. 2018. https://doi.org/10.7868/S0016794018030070

3. *Zherebtsov G.A., Pirog O.M.* Dynamics and macrostructure of ionospheric plasma / Encyclopedia of low-temperature plasma. Series B. Reference applications, databases and databanks. Volume I–3. Ionospheric plasma. Part 1. Ed. V.D. Kuznetsov, Yu.Ya. Ruzhin. M: Janus-K. P. 363–380. 2008.

4. *Kuznetsov V.D.* Space weather and risks of space activities // Space engineering and technology. No. 3 (6). P. 3–13. 2014. https://sciup.org/kosmicheskaja-pogoda-i-riski-kosmicheskoj-dejatelnosti-14343447

5. *Kurkin V.I., Polekh N.M., Zolotukhina N.A.* Ionospheric effects of weak geomagnetic storms during minimum solar activity: vernal equinox / Proceedings of the All-Russian open scientific conference Armandovskie readings: Modern problems of remote sensing, radar, wave propagation and diffraction [Electronic resource]. P. 105–114. 2022. https://doi.org/ 10.24412/2304-0297-2022-1-105-114

6. *Pilipenko V.A.* Impact of space weather on ground-based technological systems // Solar-terrestrial physics. V. 7. No. 3. P. 72–109. 2021. https://doi.org/ 10.12737/szf-73202106

7. *Podlesny A.V., Brynko I.G., Kurkin V.I., Berezovsky V.A., Kiselev A.M., Petukhov E.V.* Multifunctional chirp ionosonde for ionosphere monitoring // Heliogeophysical studies. V. 4. P. 24–31. 2013. http://vestnik.geospace.ru/index.php?id=166

8. *Polekh N.M., Zolotukhina N.A., Romanova E.B., Ponomarchuk S.N., Kurkin V.I., Podlesny A.V.* Ionospheric effects of magnetospheric and thermospheric disturbances on March 17–19, 2015 // Geomagnetism and Aeronomy. V. 56. No. 5. P. 591–605. 2016.

9. *Akasofu S.I.* Energy coupling between the solar wind and the magnetosphere // Space Sci. Rev. V. 28. N 2. P. 121–190. 1981.
https://doi.org/10.1007/BF00218810

10. *Anderson C.N.* Correlation of long wave transatlantic radio transmission with other factors affected by solar activity // Proc. Inst. Radio Eng. V. 16. N 2. P. 297−347. 1928.
https://doi.org/10.1109/JRPROC.1928.221400

11. *Borovsky J. E., Denton M. H.* Solar wind turbulence and shear: A superposed-epoch analysis of corotating interaction regions at 1 AU // J. Geophys. Res. V. 115. N A10101. 2010.
https://doi.org/10.1029/2009JA014966

12. *Buonsanto M.J.* Ionospheric storms — a review // Space Sci. Rev. V. 88. N 3–4. P. 563–601. 1999.
https://doi.org/10.1023/A:1005107532631

13. *Buresova D.*, *Lastovicka J.*, *Hejda P.*, *Bochnicek J.* Ionospheric disturbances under low solar activity conditions // Adv. Space Res. V. 54. P. 185–196. 2014.
https://doi.org/10.1016/j.asr.2014.04.007

14. *Chen Y., Liu L., Le H., Zhang H., Zhang R.* Responding trends of ionospheric F_2-layer to weaker geomagnetic activities // J. Space Weather Space Clim. V. 12. N 6. 12 pp. 2022.
https://doi.org/10.1051/swsc/2022005

15. *Ding F., Wan W., Liu L., Afraimovich E. L., Voeykov S. V., Perevalova N. P.* A statistical study of large-scale traveling ionospheric disturbances observed by GPS TEC during major magnetic storms over the years 2003–2005 // J. Geophys. Res. V.113. N A00A01. 2008.
https://doi.org/10.1029/2008JA013037

16. *Fuller-Rowell T. J., Codrescu M. V., Roble R. G., Richmond A.D.* How does the thermosphere and ionosphere react to a geomagnetic storm? / Magnetic Storms / AGU Geophysical Monograph Series. V. 98. Eds. B. T. Tsurutani, W. D. Gonzalez, Y. Kamide, J. K. Arballo. American Geophysical Union, Washington, D.C. P. 203−225. 1997.

17. *Gonzalez W. D., Joselyn J. A., Kamide Y., Kroehl H. W., Rostoker G., Tsurutani B.T., Vasyliunas V. M.* What is a geomagnetic storm? // J. Geophys. Res. V. 99. Iss. A4. P. 5771–5792. 1994.
https://doi.org/10.1029/93JA02867

18. *Goodman J.M., Ballard J.W., Patterson J.D., Gaffney B.* Practical measures for combating communication system impairments caused by large magnetic storms // Radio Sci. V. 41. N 6. RS6S41. 2006.
https://doi.org/10.1029/2005RS003404
19. *Hunsucker R.D.* Atmospheric gravity waves generated in the high-latitude ionosphere: a review // J. Geophys. Res. V. 20. N 2. P. 293−315. 1982.
20. *Kurkin V.I., Pirog O.M., Polekh N.M., Mikhalev A.V., Poddelsky I.N., Stepanov A.E.* Ionospheric response to geomagnetic disturbances in the north-eastern region of Asia during the minimum of 23rd cycle of solar activity // J. Atmos. Sol.-Terr. Phys. V. 70. N 18. P. 2346–2357. 2008.
21. *Kurkin V.I., Polekh N.M., Zolotukhina N.A.* Effect of weak magnetic storms on the propagation of hf radio waves // Geomagnetism and Aeronomy. V. 62. № 1–2. С. 104–115. 2022.
https://doi.org/ 10.1134/S0016793222020116
22. *Loewe C.A., Prolss G.W.* Classification and mean behavior of magnetic storm // J. Geophys. Res. V. 102. N A7. P. 14209–14213. 1997.
https://doi.org/ 10.1029/96JA04020
23. *Marmet P.* New digital filter for the analysis of experimental data // Rev. Sci. Instrum. V. 50. N 1. P. 79–83. 1979.
https://doi.org/ 10.1063/1.1135673
24. *Mendillo M.* Storms in the ionosphere: Patterns and processes for total electron content // Rev. Geophys. V. 44. RG4001. 2006.
https://doi.org/10.1029/2005RG000193
25. *Mikhailov A.V., Depueva A.Kh., Leschinskaya T.Yu.* Morphology of quiet time *F*2-layer disturbances: high and lower latitudes // Int. J. Geomagn. Aeron. V. 5. N 1. GI1006. 2004.
https://doi.org/ 10.1029/2003GI000058
26. *Mikhailov A.V., Perrone L., Nusinov A.A.* Mid-latitude daytime *F*2-layer disturbance mechanism under extremely low solar and geomagnetic activity in 2008–2009 // Remote Sens. 13. 1514. 2021. https://doi.org/10.3390/rs13081514
27. *Paznukhov V. V., Altadill D., Reinisch B. W.* Experimental evidence for the role of the neutral wind in the development of ionospheric storms in midlatitudes // J. Geophys. Res. V. 114. N A12319. 2009.
https://doi.org/10.1029/2009JA014479
28. *Perrone L., Mikhailov A.V., Nusinov A.A.* Daytime mid-latitude *F*2-layer Q-disturbances: A formation mechanism // Sci Rep. V. 10. 9997. 2020.
https://doi.org/10.1038/s41598-020-66134-2

29. *Pickard G. W.* The correlation of radio reception with solar activity and terrestrial magnetism // Proc. Inst. Radio Eng. V. 15. N 2. P. 83–97. 1927.
https://doi.org/10.1109/JRPROC.1927.221165
30. *Prölss G. W.* Magnetic storm associated perturbations of the upper atmosphere / Magnetic Storms / AGU Geophysical Monograph Series. V. 98. Eds. B. T. Tsurutani, W. D. Gonzalez, Y. Kamide, J. K. Arballo. American Geophysical Union, Washington, D.C. P. 227–241. 1997.
31. *Prölss G.W.* Ionospheric F-region storms: Unsolved problems / Characterizing the Ionosphere. Meeting Proc. RTO-MP-IST-056. Fairbanks, United States, 12–16 June 2006. Neuilly-sur-Seine, France. V. 10. P. 10-1–10-20. 2006.
32. *Ratovsky K.G., Klimenko M.V., Dmitriev A.V., Medvedeva I.V.* Relation of extreme ionospheric events with geomagnetic and meteorological activity // Atmosphere. V. 13. N 1. P. 146. 2022.
https://doi.org/ 10.3390/atmos13010146
33. *Tang Q., Sun H., Du Z., Zhao J., Liu Y., Zhao Z., Feng X.* Unusual enhancement of midlatitude sporadic-E layers in response to a minor geomagnetic storm // Atmosphere. V.13. N 5. P. 816. 2022.
https://doi.org/10.3390/atmos13050816
34. *Vargin P.N., Koval A.V., Guryanov V.V.* Arctic stratosphere dynamical processes in the winter 2021–2022 // Atmosphere. V.13. N 10. P.1550. 2022.
https://doi.org/10.3390/atmos13101550
35. *Zhang S-R., Vierinen J., Aa E. et al.* Tonga volcanic eruption induced global propagation of ionospheric disturbances via Lamb Waves // Front. Astron. Space Sci. 9:871275. 2022.
https://doi.org/ 10.3389/fspas.2022.871275
36. URL Intermag: https://intermagnet.org/
37. URL qd: https://wdc.kugi.kyoto-u.ac.jp/qddays/index.html
38. URL OMNI2: https://cdaweb.gsfc.nasa.gov/cdaweb/istp_public/
39. URL Oval: https://ssusi.jhuapl.edu/gal_edr-aur_cs
40. URL SME: https://supermag.jhuapl.edu/indices/

Figure captions

Fig. 1. Variations of solar wind speed *Vsw* (*a*); Akasofu parameterε (*b*); *Dst*- (*c*) and *Kr*- (*d)* indices in January 2022. Horizontal lines mark in panel (*a*), the value *Vsw* = 450 km/s, used to distinguish high-speed flows [Borovsky and Denton, 2010]; in panel (*c*), the *Dst* levels = -30 and -50 nTL, which are upper thresholds for weak and moderate magnetic storms, respectively [Loewe and Prolss, 1997]; in panel (*d*), the level *Kp* = 5, used as a lower threshold in the identification of magnetic storms. The symbols *q* and *d* with numbers indicate magnetically calm and magnetically disturbed days according to their designations in [URL qd].

Fig. 2. Map of the location of ionospheric sounding facilities and magnetic observatories. Dots show ionospheric stations and magnetic observatories; dashed and solid lines are─ radiotracks and radar beams, respectively, crosses - midpoints of radiotracks.

Fig. 3. Variations of the *Dst* index (*a*); MNF1*F2* on the Norilsk-Tory (*b*) and Magadan-Tory (*c*) routes; foF2 and *foEs* in Irkutsk (*d*). Current/background IHF1*F2* and *foF2* values are shown as black/gray lines, *foEs* values as squares.

Fig. 4. The upper panel shows the variations of the *Dst*-index; below, ΔMHF1*F2* on the Norilsk-Tory, Magadan-Tory traces and *ΔfoF2* over Irkutsk The black arrows mark the ionospheric storm elements presented in Sections 4.1, 4.2, 4.5, and 4.6 of Section 4 (see text).

Fig. 5. Variations of the corrected geomagnetic latitude of the auroral oval (gray figure) and the bottom of the ISU at longitudes 105° and 120°Å (lines), MHF1*F2* at the Norilsk-Tora and Magadan-Tora routes are shown on the left from top to bottom; on the right - a plot of the SME-index and variations of the *H-component of* the geomagnetic field recorded by three observatories located in the longitude sector under consideration. The dynamics of the SME bottom was calculated using the model [Deminov and Shubin, 2018]. The boundaries of the oval are plotted using the data given in [URL Oval].

Fig. 6. Map of auroral echo sources recorded by two SW radars at 22:15 UT on 14.01.2022. The dashed/flat lines show the position of the northern/southern boundary of the oval (plotted from the data at [URL Oval]).

Fig. 7. Variations of the *Dst*-index, ISU latitude, and short-period components of MHF1*F2* at the Magadan-Tory track and *foF2* in Irkutsk at night.

Fig. 8. Top left shows *foEs* values measured in Irkutsk during each day of January 2022; bottom shows the time of registration of *foEs* larger than 3.1 MHz. Here 3.1 MHz ─ the upper quartile of the monthly series of *foEs* values, marked in the figure by a horizontal dashed line. An ionogram containing reflections from the sporadic diffuse layer is presented on the right. It was obtained in Tora using an LFM ionosonde.

Fig. 9. (*a*) - Values of positive ΔMHF1*F2* observed on the Magadan– Torah route during each day of January 2022 (top) and the time of registration of those that lie above the upper quartiles of the monthly series of positive ΔMHF1*F2* (bottom); (*b*) - the same for negative ΔMHF1*F2* and those that lie below the lower quartiles of negative ΔMHF1*F2*. Panels (*c*) and (*d*) show similar plots plotted for positive and negative *ΔfoF2*. The horizontal dashed lines mark the upper quartiles for positive and lower quartiles for negative perturbations.

Fig. 10. Changes in the absolute deviations of *foF2* and *hmF2* from their background values are shown for positive (*a-c*) and negative (*d-e)* disturbances observed in Irkutsk in January 2022.

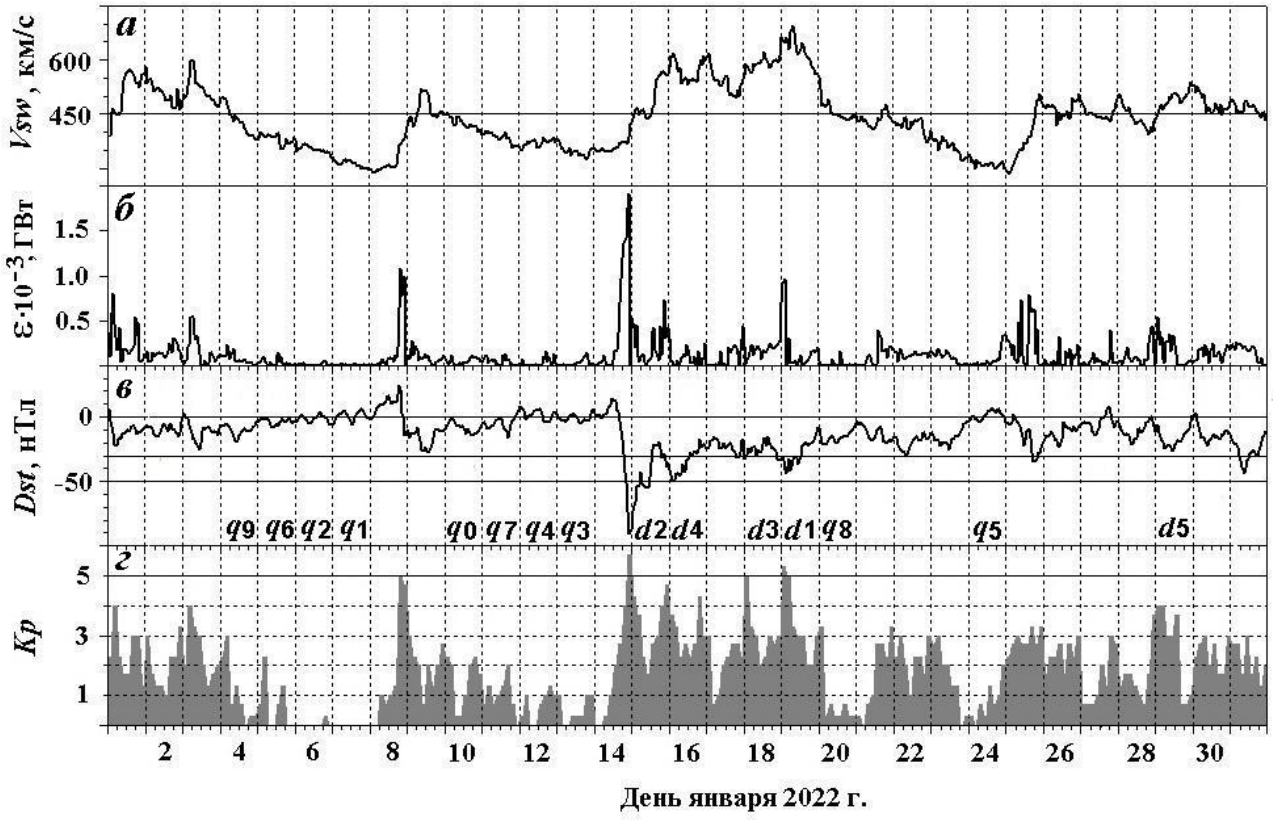

Fig. 1

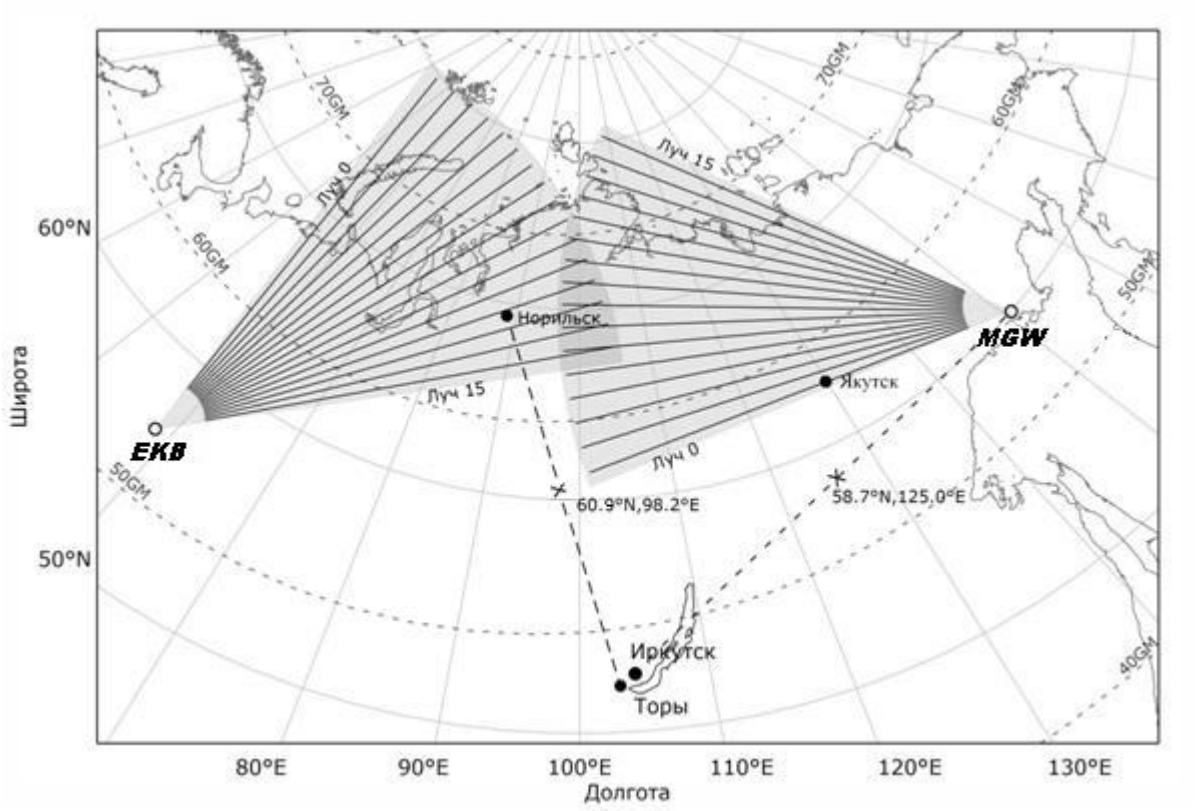
70GM
60GM
50GM
40GM
Луч 0
Луч 15
Норильск
Якутск
EKB
MGW
60.9°N,98.2°E
58.7°N,125.0°E
Иркутск
Торы
60°N
50°N
80°E
90°E
100°E
110°E
120°E
130°E
Широта
Долгота

Fig. 2

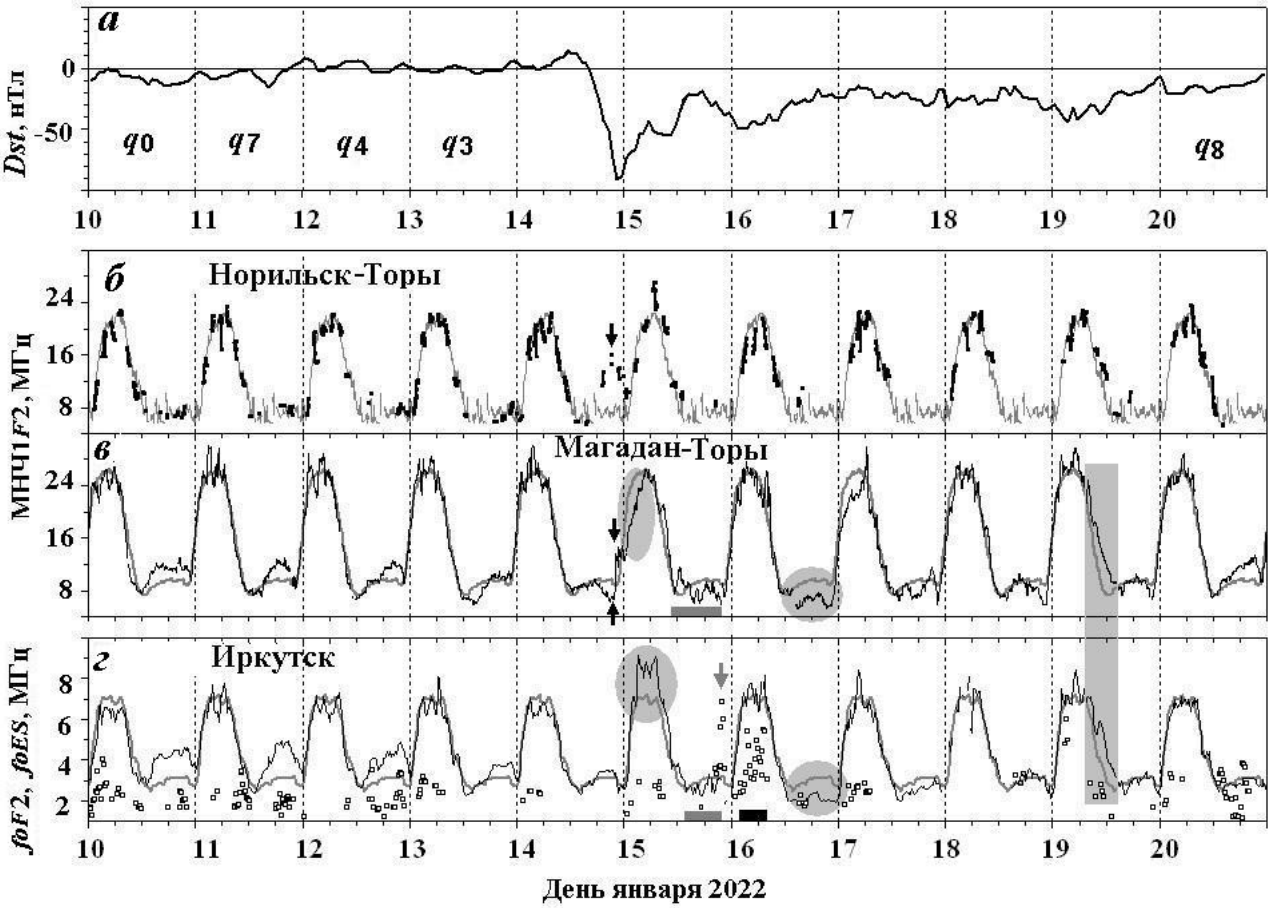
а
Dst, нТл
0
-50
q0
q7
q4
q3
q8
10
11
12
13
14
15
16
17
18
19
20
б
Норильск-Торы
в
Магадан-Торы
МНЧ1F2, МГц
24
16
8
г
Иркутск
foF2, foEs, МГц
8
6
4
2
День января 2022

Fig. 3

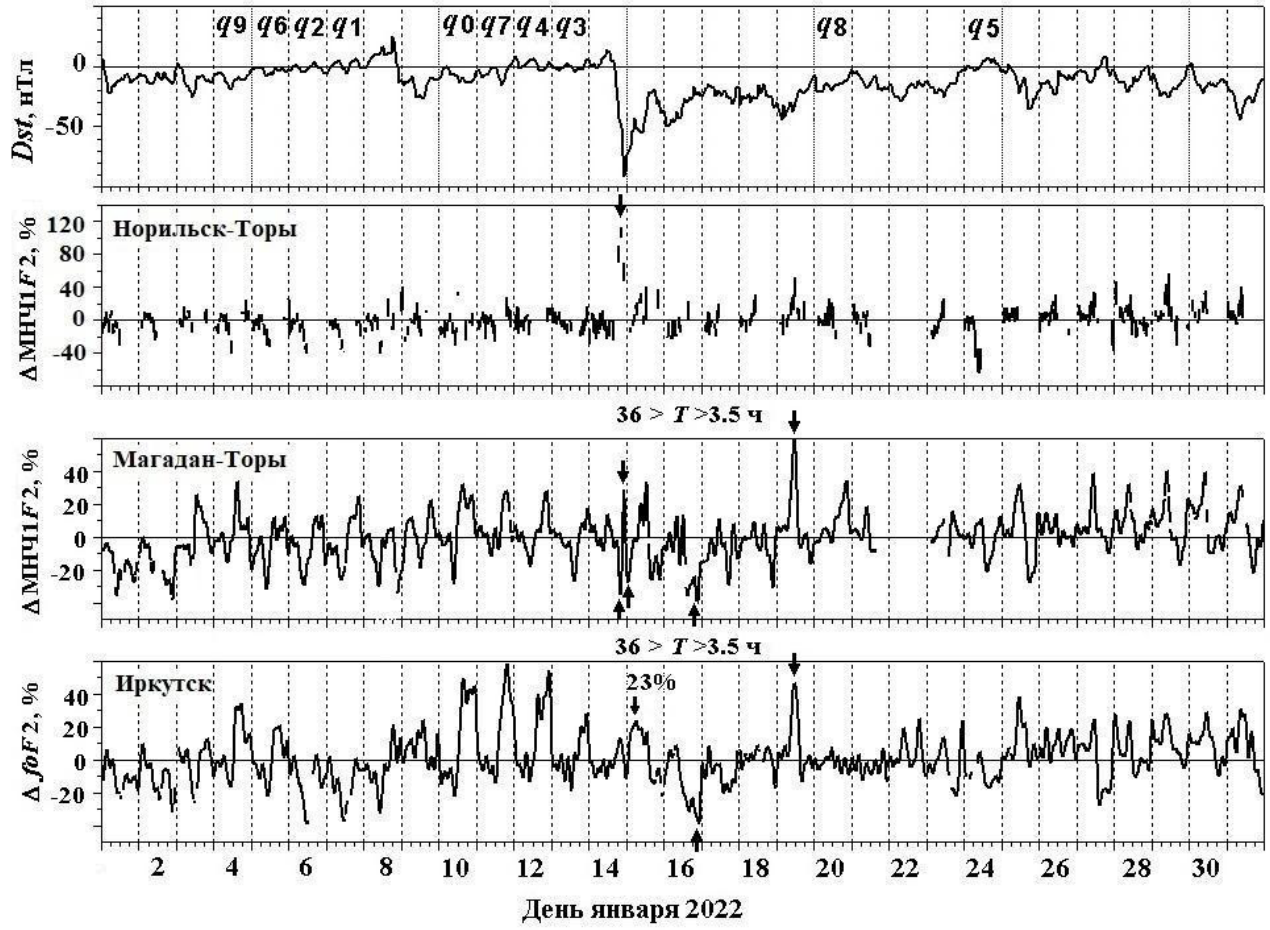
q9 q6 q2 q1
q0 q7 q4 q3
q8
q5
Dst, нТл
0
-50
Норильск-Торы
ΔМНЧ1F2, %
120
80
40
0
-40
36 > T >3.5 ч
Магадан-Торы
ΔМНЧ1F2, %
40
20
0
-20
36 > T >3.5 ч
Иркутск
23%
Δ foF2, %
40
20
0
-20
2
4
6
8
10
12
14
16
18
20
22
24
26
28
30
День января 2022

Fig. 4.

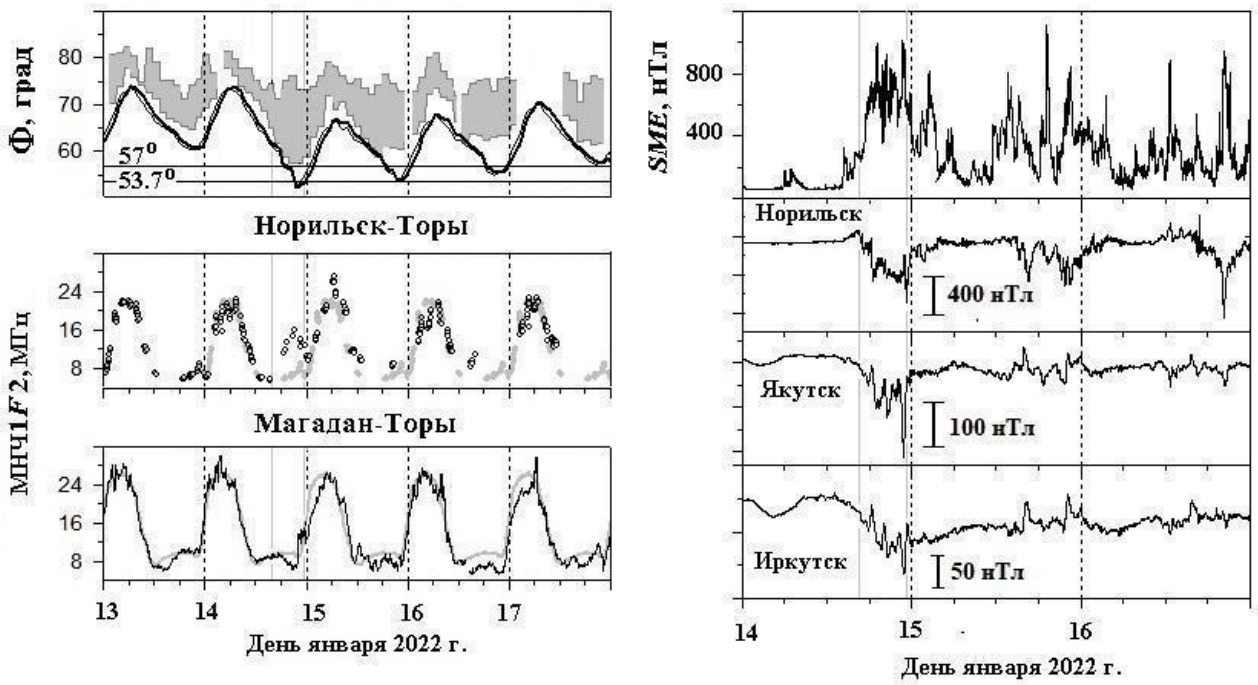
Ф, град
80
70
60
57°
53.7°
Норильск-Торы
МНЧ1F2, МГц
24
16
8
Магадан-Торы
13
14
15
16
17
День января 2022 г.
SME, нТл
800
400
Норильск
400 нТл
Якутск
100 нТл
Иркутск
50 нТл
14
15
16
День января 2022 г.

Fig. 5

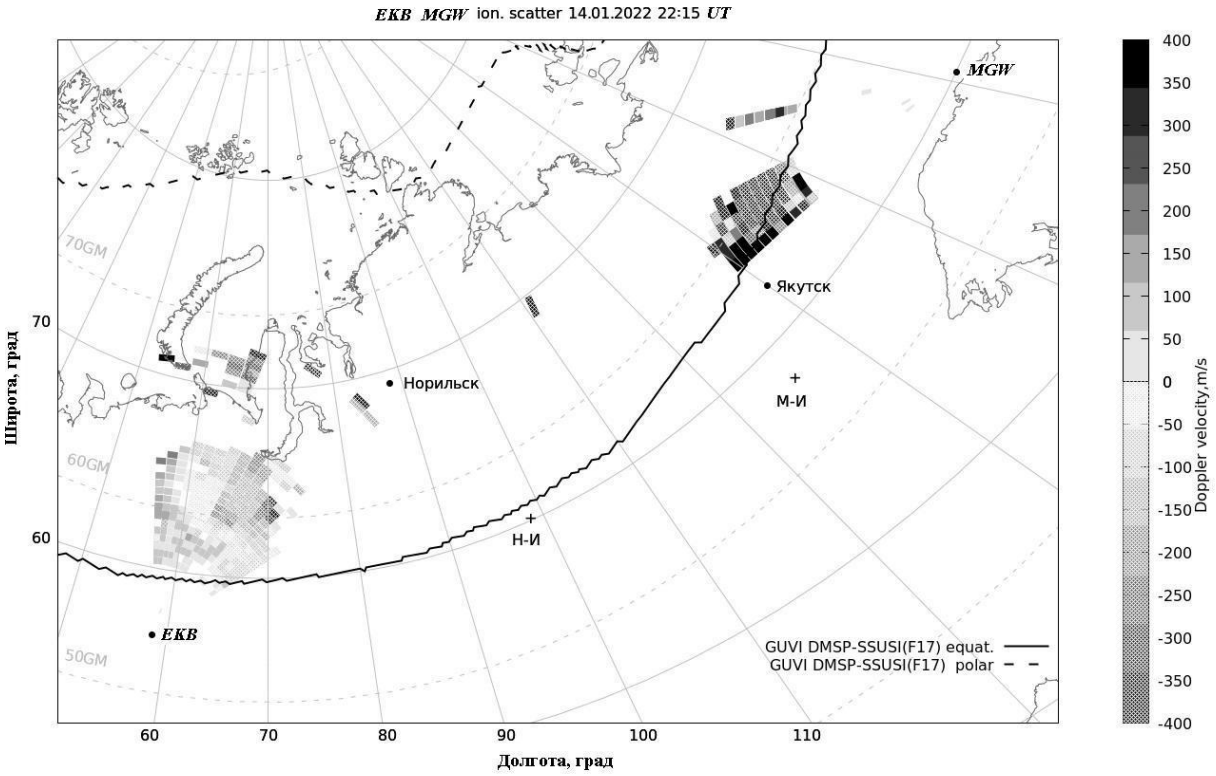
EKB MGW ion. scatter 14.01.2022 22:15 UT
MGW
Якутск
Норильск
М-И
Н-И
EKB
70GM
60GM
50GM
GUVI DMSP-SSUSI(F17) equat.
GUVI DMSP-SSUSI(F17) polar
Широта, град
Долгота, град
Doppler velocity,m/s
400
350
300
250
200
150
100
50
0
-50
-100
-150
-200
-250
-300
-350
-400
60
70
80
90
100
110

Fig. 6.

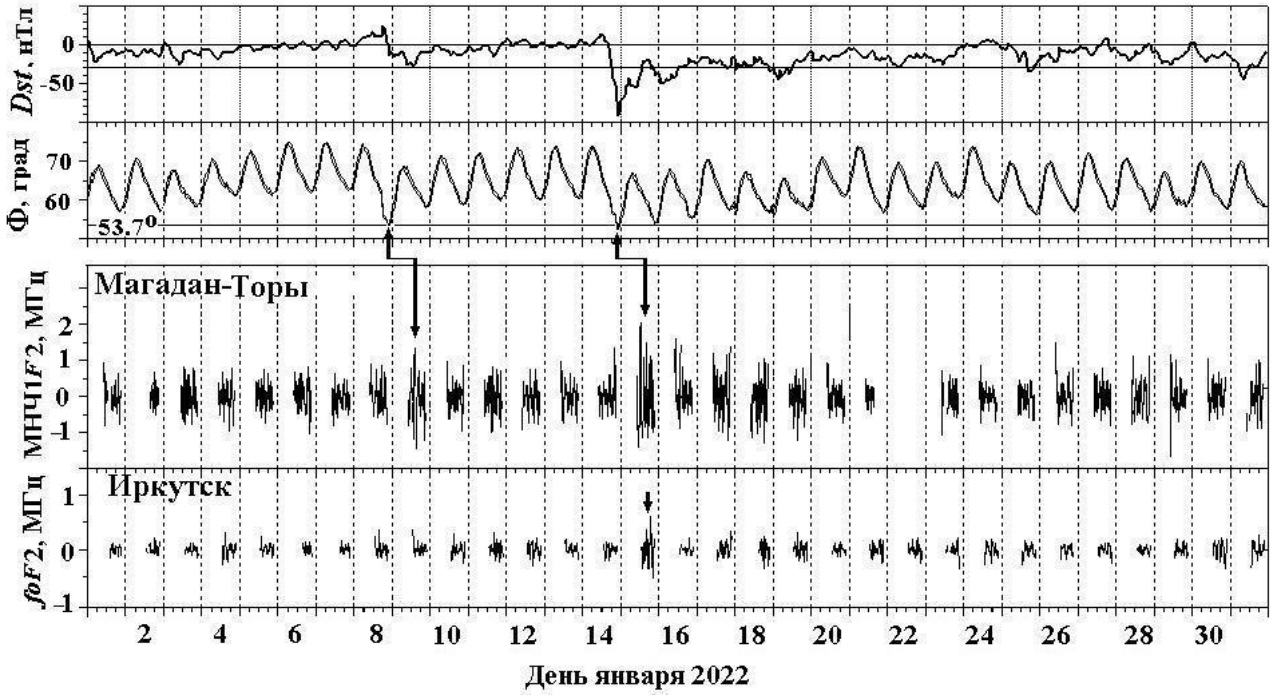
Dst, нТл
0
-50
Φ, град
70
60
53.7°
Магадан-Торы
МНЧ1F2, МГц
2
1
0
-1
Иркутск
fвF2, МГц
1
0
-1
2
4
6
8
10
12
14
16
18
20
22
24
26
28
30
День января 2022

Fig. 7.

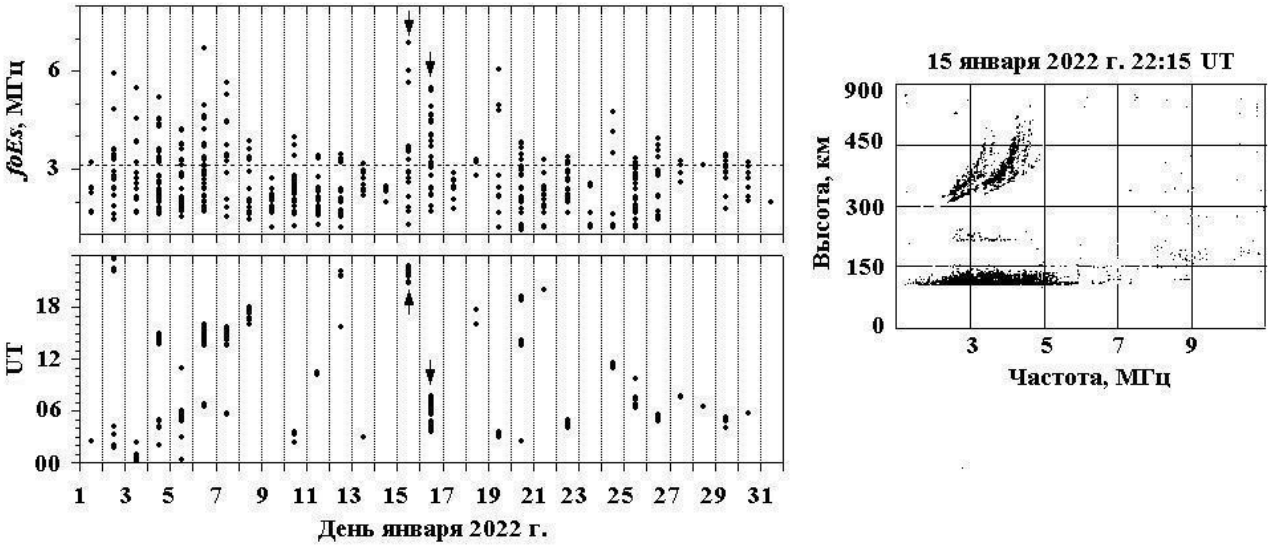
foEs, МГц
6
3
UT
18
12
06
00
1 3 5 7 9 11 13 15 17 19 21 23 25 27 29 31
День января 2022 г.
15 января 2022 г. 22:15 UT
Высота, км
900
450
300
150
0
3 5 7 9
Частота, МГц

Fig. 8.

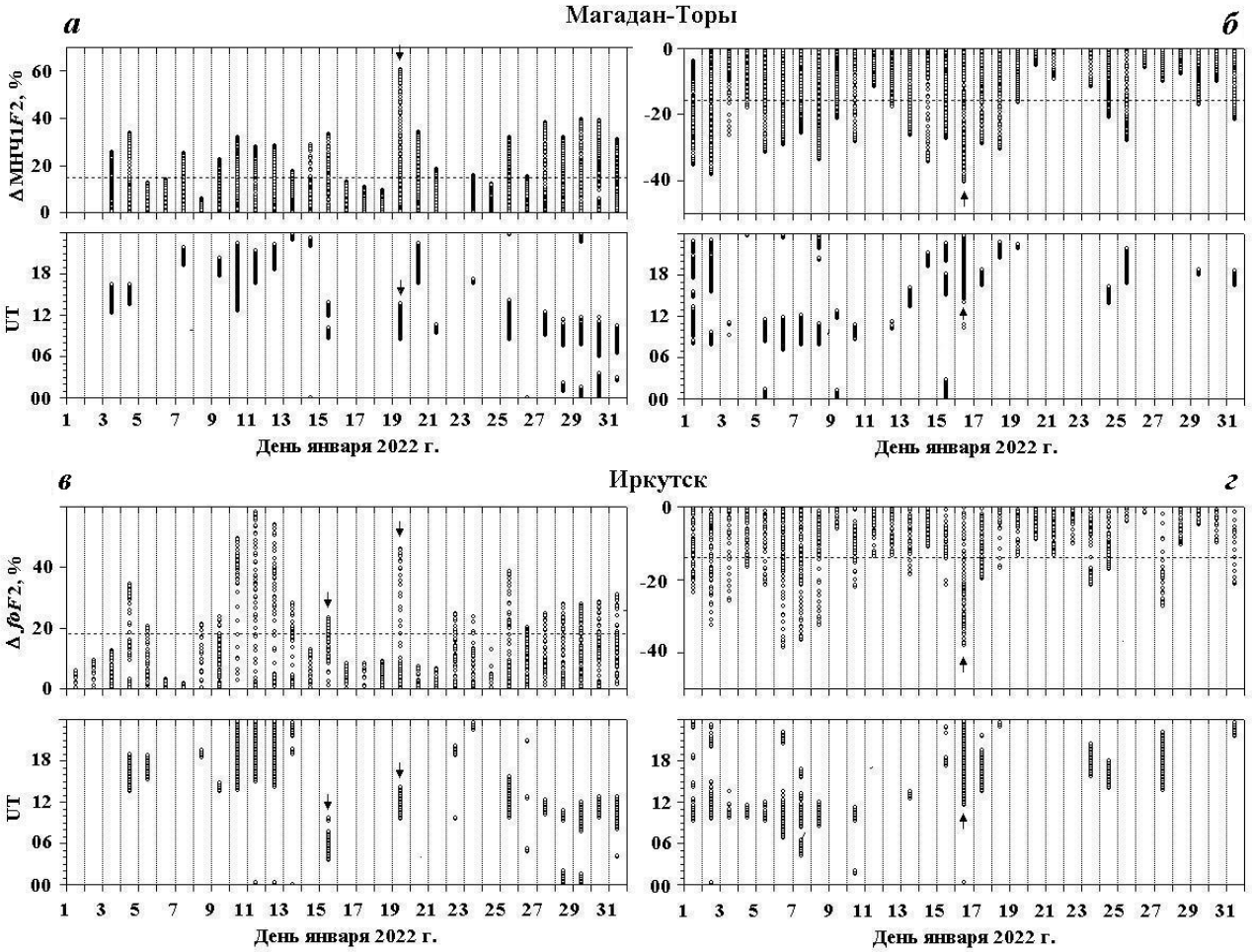
а
Магадан-Торы
б
ΔМПЧ1F2, %
UT
День января 2022 г.
в
Иркутск
г
Δ foF2, %

Fig. 9.

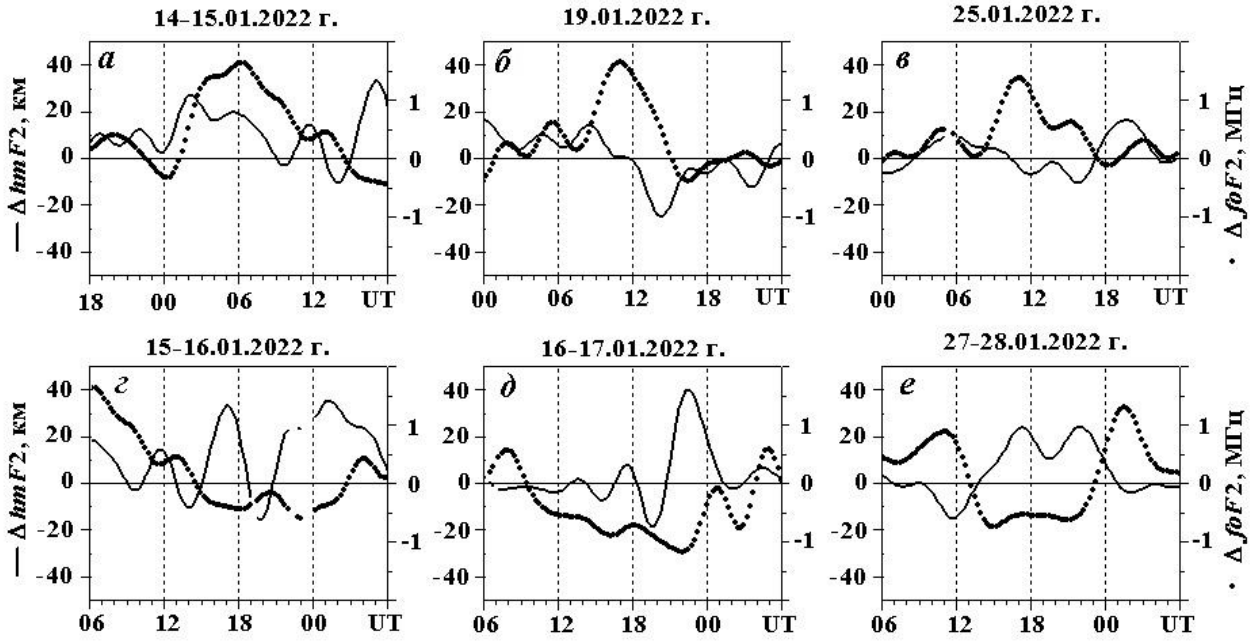
14–15.01.2022 г.
19.01.2022 г.
25.01.2022 г.
15–16.01.2022 г.
16–17.01.2022 г.
27–28.01.2022 г.
а
б
в
г
д
е
— Δ hmF2, км
• ΔfoF2, МГц
UT

Fig. 10.